JACS
JOURNAL OF THE AMERICAN CHEMICAL SOCIETY

COMMUNICATION

pubs.acs.org/JACS

Efficient Light-Harvesting Antenna with a Multi-Porphyrin Cascade

Atsuhiro Uetomo,[†] Masatoshi Kozaki,[*,†] Shuichi Suzuki,[†] Ken-ichi Yamanaka,[*,‡] Osamu Ito,[§,∥] and Keiji Okada[*,†]

[†]Graduate School of Science, Osaka City University, 3-3-138 Sugimoto, Sumiyoshi-ku, Osaka 558-8585, Japan

[‡]Toyota Central R&D Labs., Inc., 41-1, Yokomichi, Nagakute, Aichi 480-1192, Japan

[§]Fullerene Group, NIMS, 1-2-1 Sengen, Tsukuba-city, Ibaraki 305-0047, Japan

[∥]CarbonPhotoScience Laboratory, 2-1-6 Kita-Nakayama, Izumi-ku, Sendai, Miyagi 981-3215, Japan

Supporting Information

ABSTRACT: A light-harvesting antenna **1** comprising three varieties of porphyrins, each having a different number of ethynyl groups at its meso positions, was designed and synthesized. Antenna **1** exhibits intense absorption throughout the visible region up to 700 nm. Steady-state and time-resolved fluorescence studies showed that singlet-excited-state energy transfer occurs from the peripheral porphyrins to the central porphyrin with >90% efficiency and rate constants on the order of 10^{10} s^{-1}.

An essential component in an artificial photosynthetic system is a light-harvesting antenna that strongly absorbs sunlight and transfers the light energy to a reaction center with high efficiency.[1] A natural antenna system generally possesses several types of antenna pigments, which help in collecting photons with energies across the visible region. Moreover, these pigments are systematically arranged to form a lowest-excited-state energy gradient that enhances the efficiency of energy transfer.[1,2] Both the magnitude of the absorbance cross section in the visible region and the energy-transfer efficiency are essential factors in determining the light-harvesting ability of the antenna.[3] Porphyrins exhibit strong absorption in the visible region, making them important chromophores for the construction of artificial light-harvesting antennae.[4] To date, a large number of porphyrin assemblies that act as antennae with highly efficient energy transfers have been constructed with a combination of free-base and Zn porphyrins as the energy acceptors and donors, respectively.[5,6] However, these porphyrin antennae display the desired intense absorption in only a limited portion of the visible region, and as a consequence, their light-harvesting ability is restricted. Herein we report the novel light-harvesting antenna **1** (Figure 1), which strongly absorbs light across the 400−700 nm region with $\varepsilon >$ 56 000 M^{-1} cm^{-1} and exhibits highly efficient energy transfer from the peripheral porphyrins to the central porphyrin.

Antenna **1** has three different Zn porphyrins: eight tetraphenyl Zn porphyrin units (**TP-Por**), four Zn porphyrin units with two *meso*-ethynyl and two *meso*-phenyl groups (**DE-Por**), and a Zn porphyrin unit with four *meso*-ethynyl groups (**TE-Por**) (Figure 1). The direct connection of ethynyl groups to the meso positions of the porphyrin results in a considerable red shift of the absorption bands.[7] Therefore, the energy of the lowest excited state decreases in the order **TP-Por** > **DE-Por** > **TE-Por**. These porphyrins are arranged in a dendritic architecture in **1** in order to facilitate the transfer of the excitation energy from the peripheral porphyrins (**TP-Por** and **DE-Por**) to the central porphyrin (**TE-Por**). **DE-Por** is located at the terminal of the phenylene ethynylene conjugated chain, whereas **TP-Por** is linked through nonconjugated benzyl ether chains. For this reason, **DE-Por** could be expected to function not only as a light absorber but also as a mediator in energy transfer from **TP-Por*** to **TE-Por**.

Antenna **1** was synthesized according to the previously reported convergent method (Scheme 1).[8] Pinacol borate **3** with a **TP-Por** terminal was connected to **DE-Por**-terminated conjugated chain **2** using a Suzuki−Miyaura coupling reaction, which afforded compound **4** in quantitative yield.[9] After incorporation of an iodo group to give **5**,[10] a copper-free Sonogashira coupling reaction with **6** provided antenna **1**.[11] The crude product was purified by cycling gel-permeation chromatography to afford **1** in 17% yield. Antenna **1** was highly soluble in organic solvents such as tetrahydrofuran (THF) and dichloromethane and was unambiguously characterized by means of NMR and MALDI−TOF mass spectrometry experiments.

Antenna **1** in THF exhibits characteristic bands due to the component porphyrins (Figure 2). Three intense absorption bands at λ_{max} (log ε) = 426 nm (6.69), 453 nm (6.23), and 498 nm (5.85) were assigned to Soret bands attributed to **TP-Por**, **DE-Por**, and **TE-Por**, respectively, on the basis of comparisons to the spectra of **3**, **2**, and **7**. In addition, a series of weak Q bands with maxima at λ_{max} = 557 nm (5.28), 598 nm (5.12), 653 nm (5.56), and 697 nm (5.11) were observed as an overlap of absorptions of **TP-Por**, **DE-Por**, and **TE-Por** on the basis of the spectra of **3**, **2**, and **7**, respectively (Figure 2 inset). Although the observed absorption spectrum of the antenna **1** could be roughly simulated using the spectra of the reference compounds **2**, **3**, and **7** [Figure S1 in the Supporting Information (SI)], there were modest differences between observed and simulated spectra. These results suggest weak electronic interactions between the porphyrin units in the ground state. Antenna **1** has strong absorptions across the 400−700 nm region with $\varepsilon >$ 56 000 M^{-1} cm^{-1}. Furthermore, the absorption spectral shape of **1** is roughly similar to the solar spectrum. Because of these characteristic shapes of the absorption and emission spectra (see below), selective excitation of **TP-Por**, **DE-Por**, and **TE-Por** in **1** and detection and identification of the emitting porphyrin were possible.

Received: June 1, 2011
Published: July 26, 2011

dx.doi.org/10.1021/ja2050343 | *J. Am. Chem. Soc.* 2011, 133, 13276–13279

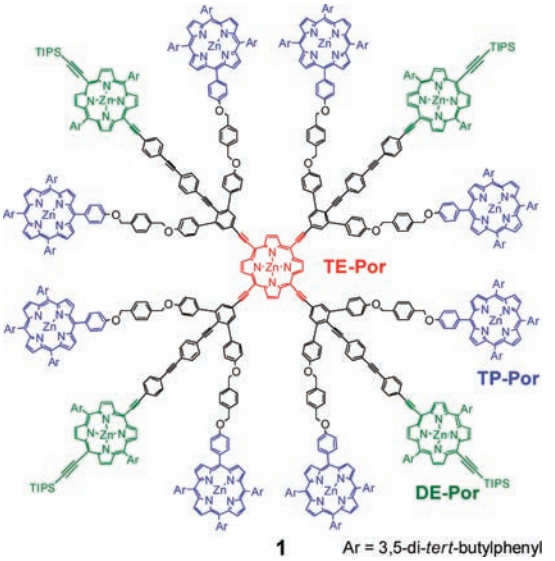

Figure 1. Chemical structure of light-harvesting antenna **1**.

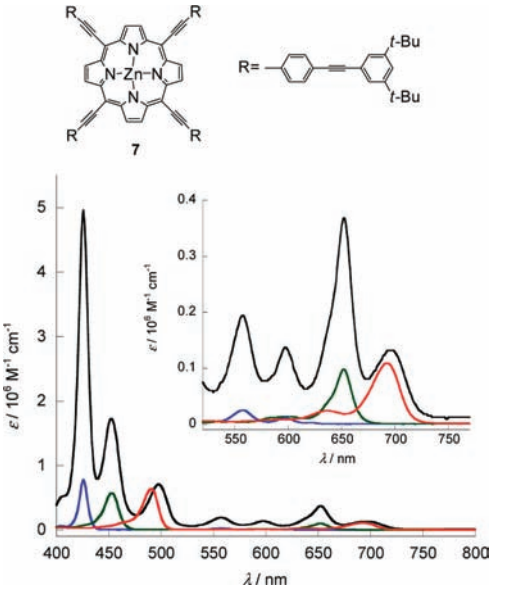

Figure 2. Absorption spectra of **1** (black), **2** (green), **3** (blue), and **7** (red) measured in THF. The inset shows expanded absorption spectra in the Q-band region.

Scheme 1

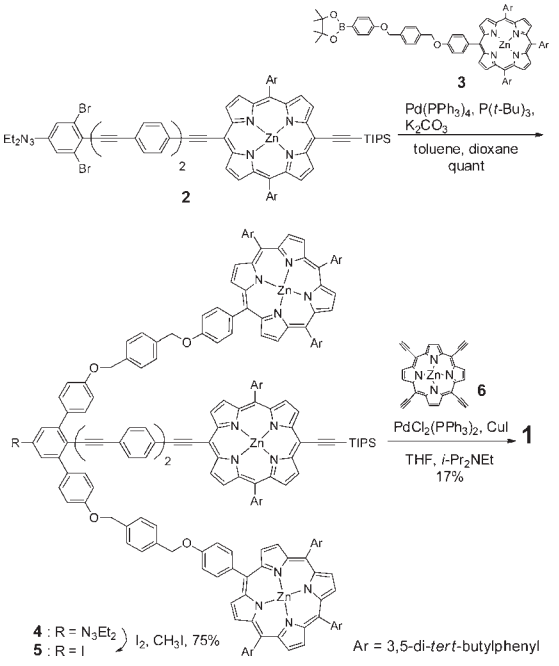

To evaluate the efficiency of singlet-excited-state energy transfer from **TP-Por*** to **TE-Por** and from **DE-Por*** to **TE-Por**, steady-state fluorescence quenching in **1** was investigated with model compounds **2** and **3** in degassed THF. The excitation of **TP-Por** in **3** and **DE-Por** in **2** showed characteristic fluorescence spectra for the two porphyrin units at $\lambda_{EM\text{-}max}$ = 604 and 656 nm for **3** and 656 and 717 nm for **2** with quantum yields of 0.033 and 0.16, respectively (Figure 3). Selective excitation of **TP-Por** in **1** at 426 nm, at which wavelength the incident light is absorbed by **TP-Por** and **DE-Por** with an absorption (I) ratio of I(**TP-Por**):I(**DE-Por**) = 23:1, resulted in the appearance of an intense emission with $\lambda_{EM\text{-}max}$ = 707 and 780 nm (Figure 3a). The quantum yield of the emission was determined to be 0.14 by the absolute method.[12] The observed fluorescence spectral shape was successfully simulated using component fluorescence patterns from **2** and **3**, showing that the observed fluorescence can be divided into three components with **TE-Por**:**DE-Por**:**TP-Por** area ratios of 91:7:1 (Figure S2). Thus, selective excitation of **TP-Por** gave **TE-Por*** with 91% quantum efficiency for the energy transfer and a fluorescence quantum efficiency (Φ_f) of 0.13 for the acceptor chromophore **TE-Por**. Similarly, selective excitation of **DE-Por** at 455 nm, at which wavelength I(**DE-Por**):I(**TE-Por**) = 30:1, gave a fluorescence pattern similar to that for **TE-Por** with a quantum yield of 0.13, accompanied by fluorescence quenching of **DE-Por** (Figure 3b). The observed fluorescence spectrum was reconstructed from two components with a **TE-Por**:**DE-Por** area ratio of 94:6 (Figure S3), indicating selective singlet energy transfer from **DE-Por*** to **TE-Por** with 94% quantum efficiency for the energy transfer and Φ_f = 0.12 for the acceptor chromophore **TE-Por**. The fluorescence quantum yields in these intramolecular energy transfers are in good agreement with the quantum yield (0.13) for direct excitation of **TE-Por** in **1**. Because of the smaller loss during energy transfer and stronger absorptions of **1** in the visible region, the fluorescence from **TE-Por*** in **1** should be much greater in intensity than that of **7** when the samples are exposed to the same intensity of visible light.

The dynamic processes involved in the energy transfer were investigated using time-resolved fluorescence spectroscopy.[13] The singlet-excited-state energy transfer in **1** involves three processes: **TP-Por*** to **DE-Por** (EN1), **TP-Por*** to **TE-Por** (EN2), and **DE-Por*** to **TE-Por** (EN3). First, for simpler analysis, we measured the rate constants of energy transfer (k_{EN}) for the model compounds **4**, **8**, and **9** (Figure 4), which have the least fluorescence overlap, to obtain approximate values for the energy-transfer rates for EN1, EN2, and EN3, respectively. The k_{EN} values for EN1 and EN2 are similar and on the order of 10^9 s^{-1}, and the value for step EN3 is ~10 times larger than those for EN1 and EN2 (Table 1). These rate constants are roughly reproduced by the Förster equation (Table S2 in the SI),[14] although the participation of the superexchange mechanism thorough conjugated bridges cannot be excluded.[15]

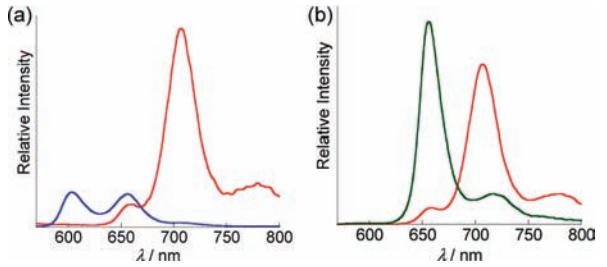

Figure 3. Steady-state fluorescence spectra of (a) **1** (red) and **3** (blue) (λ_{ex} = 426 nm) and (b) **1** (red) and **2** (green) (λ_{ex} = 453 nm) measured in THF. Fluorescence intensities were measured after normalizing the absorbance at the excitation wavelength.

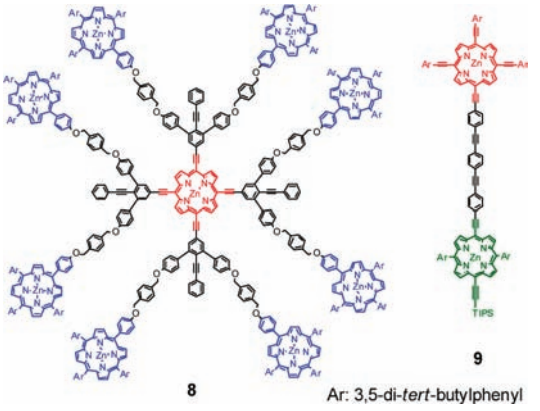

Figure 4. Chemical structures of reference compounds **8** and **9**.

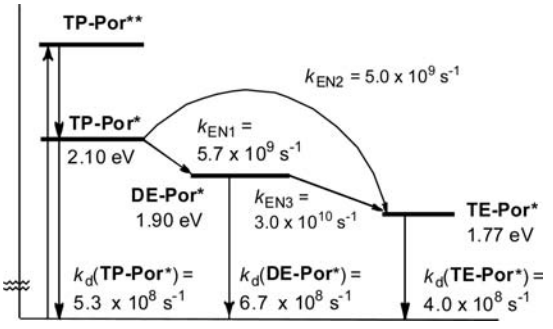

Figure 5. Energy diagram and relaxation process from excited states of **TP-Por** in antenna **1**. * and ** denote the first and second excited states, respectively.

Selective excitation of **TP-Por** (λ_{ex} = 427 nm) in **1**, which has two possible EN routes, gave a fluorescence decay (λ_{detect} = 610 nm, **TP-Por***) with $k_{EN} = 1.2 \times 10^{10}$ s^{-1}. As expected, the k_{EN} value is very close to the sum of those obtained from the model compounds, suggesting that the EN1 and EN2 processes with similar rate constants occur concurrently in **1**. Excitation of **DE-Por** (λ_{ex} = 456 nm) in **1** gave a major fluorescence decay (λ_{detect} = 660 nm, **DE-Por***) with $k_{EN} = 3.0 \times 10^{10}$ s^{-1} for EN3,[16] which is in good agreement with the values estimated from model compound **9**. These decay parameters of **TP-Por***, **DE-Por***, and **TE-Por*** in **1** are summarized in Figure 5. The decay rate constants without energy transfer (k_d) were determined using model compounds **3** (λ_{ex} = 427 nm, λ_{detect} = 610 nm, $k_d = 5.3 \times 10^8$ s^{-1}) for **TP-Por*** and **2** (λ_{ex} = 456 nm, λ_{detect} = 660 nm, $k_d = 6.7 \times 10^8$ s^{-1}) for **DE-Por*** and using a longer decay constant in **1** (λ_{ex} = 456 nm, λ_{detect} = 710 nm, $k_d = 4.0 \times 10^8$ s^{-1}) for **TE-Por***. From these rate parameters, the following quantum efficiencies of energy transfer were calculated: 51 and 45% from **TP-Por*** to **DE-Por** and **TE-Por**, respectively (giving a total quantum efficiency of 96%) and 98% from **DE-Por*** to **TE-Por**. The rapid energy transfer from **DE-Por*** to **TE-Por** plays an important role (~50% contribution) in this cascade process by mediating the transfer of excitation energy from **TP-Por*** to **TE-Por**.

Table 1. Photophysical Data for 1, 4, 8, and 9 in THF

	λ_{ex}/nm	λ_{detect}/nm	k_{EN}/s^{-1}	energy-transfer step
1	427	610	1.2×10^{10}	EN1 + EN2
4	427	610	5.7×10^9	EN1
8	427	610	5.0×10^9	EN2
1	456	660	3.0×10^{10}	EN3
9	456	660	3.0×10^{10}	EN3

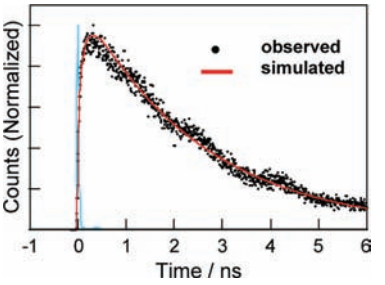

Figure 6. Fluorescence decay curve at 710 nm of **1** excited at 427 nm in THF (dots). The red solid line was obtained by the simulation using eq 1. The shape decay (blue) is the laser pulse profile.

Finally, we analyzed the fluorescence decay at 710 nm after selective excitation of **TP-Por** (λ_{ex} = 427 nm) using the determined rate parameters in Table 1. **TE-Por*** has a strong fluorescence intensity at 710 nm; however, **DE-Por*** and **TP-Por*** also have weak fluorescence intensities at this wavelength. Obviously, **TE-Por*** is generated via all three steps EN1−EN3. According to the kinetic model (see the SI), the time dependence should be expressed by eq 1:[17]

$$I(t) = a\exp\{-[k_{EN1} + k_{EN2} + k_d(\textbf{TP-Por*})]t\} + b\exp\{-[k_{EN3} + k_d(\textbf{DE-Por*})]t\} + c\exp[-k_d(\textbf{TE-Por*})t] \quad (1)$$

With the values in Figure 5, the observed decay curve at 710 nm was successfully simulated using the parameters $a = -0.32$, $b = 0.10$, and $c = 0.58$ (Figure 6). Furthermore, the time-dependent contributions of the excited states of **TP-Por***, **DE-Por***, and **TE-Por*** were clarified (Figure S12). These features are completely consistent with highly efficient energy transfer in **1**.

In conclusion, we have synthesized a novel light-harvesting antenna in which three kinds of porphyrins with different numbers of ethynyl groups at the meso positions are precisely located. Strong absorption throughout the visible region and nearly quantitative energy transfer from the peripheral porphyrins to the central porphyrin were observed. In addition, it should be noted that the benzyl ether chains in the antenna **1** could easily be replaced by dendritic structures, which would be advantageous

for the construction of light-harvesting systems with large numbers of chromophores. These results prove that the synthesis of porphyrin dendrimers using snowflake architectures is a valuable tool for the construction of artificial light-harvesting antennae.

■ ASSOCIATED CONTENT

Supporting Information. Detailed synthetic procedures and spectral data. This material is available free of charge via the Internet at http://pubs.acs.org.

■ AUTHOR INFORMATION

Corresponding Author
kozaki@sci.osaka-cu.ac.jp; yamanaka@mosk.tytlabs.co.jp; okadak@sci.osaka-cu.ac.jp

■ ACKNOWLEDGMENT

This work was partially supported by Grants 23350022 and 22350066 from JSPS. We thank for Otsuka Electronics for measurements of fluorescence quantum yields.

■ REFERENCES

(1) (a) Barber, J.; Andersson, B. *Nature* **1994**, *370*, 31. (b) Umena, Y.; Kawakami, K.; Shen, J.-R.; Kamiya, N. *Nature* **2011**, *473*, 55. (c) Blankenship, R. E. *Molecular Mechanism of Photosynthesis*; Blackwell Science: Oxford, U.K., 2002.

(2) Devadoss, C.; Bharathi, P.; Moore, J. S. *J. Am. Chem. Soc.* **1996**, *118*, 9635.

(3) (a) Hippius, C.; van Stokkum, I. H. M.; Gsänger, M.; Groeneveld, M. M.; Williams, R. E.; Würthner, F. *J. Phys. Chem. C* **2008**, *112*, 2476. (b) Diring, S.; Puntoriero, F.; Nastasi, F.; Campagna, S.; Ziessel, R. *J. Am. Chem. Soc.* **2009**, *131*, 6108.

(4) (a) Harvey, P. D.; Stern, C.; Guilard, R. Bio-inspired Molecular Devices Based on Systems Found in Photosynthetic Bacteria. In *Handbook of Porphyrin Science*; Kadash, K. M., Smith, K. M., Guilard, R., Eds.; World Scientific: San Diego, CA, 2000; Vol. 11, Chapter 49, pp 1−179. (b) Imahori, H. *J. Phys. Chem. B* **2004**, *108*, 6130. (c) Satake, A.; Kobuke, Y. *Tetrahedron* **2005**, *61*, 13.

(5) (a) Aratani, N.; Kim, D.; Osuka, A. *Acc. Chem. Res.* **2009**, *42*, 1922. (b) Kozaki, M.; Uetomo, A.; Suzuki, S.; Okada, K. *Org. Lett.* **2008**, *10*, 4477. (c) Choi, M.; Aida, T.; Yamazaki, T.; Yamazaki, I. *Angew. Chem., Int. Ed.* **2001**, *40*, 3194. (d) Li, J.; Ambroise, A.; Yang, S. I.; Diers, J. R.; Seth, J.; Wack, C. R.; Bocian, D. F.; Holten, D.; Lindsey, J. S. *J. Am. Chem. Soc.* **1999**, *121*, 8927.

(6) For light-harvesting antenna containing varieties of porphyrins, see: (a) Song, H.-E.; Kirmaier, C.; Schwartz, J. K.; Hindin, E.; Yu, L.; Bocian, D. F.; Lindsey, J. S.; Holten, D. *J. Phys. Chem. B* **2006**, *110*, 19131. (b) Nakano, A.; Osuka, A.; Yamazaki, I.; Yamazaki, T.; Nishimura, Y. *Angew. Chem., Int. Ed.* **1998**, *37*, 3023.

(7) (a) Lin, V. S.-Y.; DiMagno, S. G.; Therien, M. J. *Science* **1994**, *264*, 1105. (b) Taylor, P. N.; Huuskonen, J.; Rumbles, G.; Aplin, R. T.; Williams, E.; Anderson, H. L. *Chem. Commun.* **1998**, 909. (c) Nakano, A.; Osuka, A.; Yamazaki, T.; Nishimura, Y.; Akimoto, S.; Yamazaki, I.; Itaya, A.; Murakami, M.; Miyasaka, H. *Chem.—Eur. J.* **2001**, *7*, 3134.

(8) (a) Kozaki, M.; Okada, K. *Org. Lett.* **2004**, *6*, 485. (b) Kozaki, M.; Akita, K.; Okada, K. *Org. Lett.* **2007**, *9*, 1509. (c) Kozaki, M.; Akita, K.; Okada, K. *Org. Lett.* **2007**, *9*, 3315.

(9) Miyaura, N.; Suzuki, A. *Chem. Rev.* **1995**, *95*, 2457.

(10) (a) Moore, J. S.; Weinstein, E. J.; Wu, Z. *Tetrahedron Lett.* **1991**, *32*, 2465. (b) Wu, Z.; Moore, J. S. *Tetrahedron Lett.* **1994**, *35*, 5539.

(11) (a) Sonogashira, K.; Tohda, Y.; Hagihara, N. *Tetrahedron Lett.* **1975**, *16*, 4467. (b) Wagner, R. W.; Ciringh, Y.; Clausen, C.; Lindsey, J. S. *Chem. Mater.* **1999**, *11*, 2974.

(12) Absolute quantum yields of the fluorescence were measured using an Otsuka Electronics QE-1100 spectrometer with an MCPD-9800 detector.

(13) Yamanaka, K.; Okada, T.; Goto, Y.; Tani, T.; Inagaki, S. *Phys. Chem. Chem. Phys.* **2010**, *12*, 11688.

(14) Lakowicz, J. R. *Principles of Fluorescence Spectroscopy*, 3rd ed.; Springer: New York, 2006.

(15) Pettersson, K.; Kyrychenko, A.; Rönnow, E.; Ljungdahl, T.; Mårtensson, J.; Albinsson, B. *J. Phys. Chem. A* **2006**, *110*, 310.

(16) Minor decay components were observed because of the fluorescence overlaps at 660 nm (**TP-Por*** and **TE-Por***): $\tau \approx 240$ ps (20%) and 1.9 ns (12%).

(17) The reverse energy-transfer processes from **DE-Por*** to **TP-Por** and from **TE-Por*** to **TP-Por** (or **DE-Por**) (EN1R−3R in Table S2) may occur because of the small energy gaps between these excited states (Figure 5). The Förster mechanism suggests that the reverse energy-transfer rate constants are approximately one-tenth of those for the forward reactions (Table S2). To avoid overparametrization and ensure their reliability for analysis, we treated the decay data using the consecutive reaction scheme without these reverse energy transfers.